İSTANBUL TECHNICAL UNIVERSITY ★ EURASIA INSTITUTE OF EARTH SCIENCES

MODELLING OF EARTHQUAKE HISTORY OF THE KNIDOS FAULT ZONE USING IN SITU CHLORINE-36 SURFACE EXPOSURE DATING

M.Sc. THESIS

Sefa ŞAHİN

Department of Climate and Marine Sciences

Earth System Science Programme

Thesis Advisor: Assoc. Prof. Dr. Cengiz YILDIRIM

DECEMBER 2015

İSTANBUL TECHNICAL UNIVERSITY ★ EURASIA INSTITUTE OF EARTH SCIENCES

MODELLING OF EARTHQUAKE HISTORY OF THE KNIDOS FAULT ZONE USING IN SITU CHLORINE-36 SURFACE EXPOSURE DATING

M.Sc. THESIS

Sefa ŞAHİN
(601112010)

Department of Climate and Marine Sciences

Earth System Science Programme

Thesis Advisor: Assoc. Prof. Dr. Cengiz YILDIRIM

DECEMBER 2015

İSTANBUL TEKNİK ÜNİVERSİTESİ ★ AVRASYA YER BİLİMLERİ ENSTİTÜSÜ

KNİDOS FAY ZONU'NUN DEPREM GEÇMİŞİNİ KLOR-36 YÜZEY YAŞ TAYİNİ YÖNTEMİYLE MODELLEME

YÜKSEK LİSANS TEZİ

Sefa ŞAHİN
(6011212010)

İklim ve Deniz Anabilim Dalı

Yer Sistem Bilimi

Tez Danışmanı: Doç. Dr. Cengiz YILDIRIM

ARALIK 2015

Sefa ŞAHİN, a M.Sc. student of ITU Eurasia Institute of Earth Science student ID 601112010, successfully defended the dissertation entitled "Modelling of Earthquake History of the Knidos Fault Zone Using *in situ* Chlorine-36 Surface Exposure Dating", which he prepared after fulfilling the requirements specified in the associated legislations, before the jury whose signatures are below.

Thesis Adviros:	**Assoc. Prof. Dr. Cengiz YILDIRIM** Istanbul Technical University	.....
Jury Members:	**Assoc. Prof. Dr. M. Akif SARIKAYA** Istanbul Technical University	.....
	Asst. Prof. Dr. Tolga GÖRÜM Istanbul University	.....

Date of Submission : 26.11.2015

Date of Defence : 22.03.2016

To anyone who has been struggling with using this thesis format,

FOREWORD

First of all, I would like to thank all of professors and students at Eurasia Institute of Earth Science who have supported me. Especially, I am grateful to my supervisor, Assoc. Prof. Dr. Cengiz YILDIRIM for sincere academic support and showing me the different point of view in earth science and guidance during these three years.I also wish to thank Assoc. Prof. Dr. M.Akif SARIKAYA and Prof. Dr. Attila ÇİNER, who are always eager to help us anytime both office and field works. I also would like to thank Dr. Lucilla BENEDETTI for crucial discussion and her precious experiences and what's more her hospitality when I was at CEREGE, Aix-en-Provence in France. I want to thanks her student Jim Tesson showing me the important details about the modeling approach.

I owe my appreciation to my friend and colleague Asen SABUNCU for all of his contribution for programing and brainstorm which we had. My mountaineer friend Uğur KIROĞLU who helped us for sampling of materials and made this very difficult process us to feasible, safe and entertaining. I want to thank Oğuzhan KÖSE and Savaş GÜNDÜZ for all of their help that we did at Kozmo-Lab in Fatih University. Many thanks to Dr. Orkan ÖZCAN providing remote sense data which he provided. This study could not have been possible without their invaluable assistance and encouragement. I feel fortunate to have had a chance to work with them.

Most importantly, I want to give my special thanks to my parents and my elder brother and sister and my fiancee. Thank you very much for your endless supports and allowing me to follow my ambitions.

This thesis is prepared as a part of the research project entitled "Determination of Recurrence Intervals of Earthquakes and Slip Rates of the Knidos Fault Using Cosmogenic Chlorine-36 Surface Dating"(Project No: 113Y436) of the Scientific and Technological Research Council of Turkey (TÜBİTAK). I wish to give all my appreciation for their financial support.

December 2015

Sefa ŞAHİN
Geophsysic Engineer

TABLE OF CONTENTS

Page

ABBREVIATIONS

AIC	: Akaike Information Criteria
AMS	: Accelerated Mass Spectrometer
RMS	: Root Mean Square
RMSw	: Root Mean Square weighted

SYMBOLS

α	: Colluvial wedge dip
β	: Fault scarp dip
θ	: Upper part of scarp dip
γ	: Inclination angle
Φ	: Azimuth angle

LIST OF TABLES

Page

LIST OF FIGURES

Page

MODELLING OF EARTHQUAKE HISTORY OF THE KNIDOS FAULT ZONE USING IN SITU CHLORINE-36 SURFACE EXPOSURE DATING

SUMMARY

Knidos is an ancient city, which is located in the south of Gulf of Gökova in Western Anatolia. The Knidos Fault Zone is situated in ancient settlement ruins on the Datça Peninsula. The recent geological and archaeological evidences point out that this ancient site has been affected by at least two crucial momentous seismic events. In the light of this information, we have carried out cosmogenic 36Cl dating in order to obtain information about the seismic history of the Knidos Fault Zone. Using cosmic-ray surface exposure dating of a well-preserved limestone fault scarp facilitates us to attain information, which reveals a seismic history of faulting events and identifies timing and recurrence interval of past major earthquakes, and slip rates of the Knidos Fault Zone. There are two distinct faults located in the study area; those are the Demeter Fault and the Mezarlık Fault. I have chosen to aim at the Mezarlık Fault on account of that it has well-preserved fault scarp. The concentration of cosmogenic ^{36}Cl isotopes measured in 128 limestone samples from a ~15m high bedrock fault scarp helps us to reveal the fault displacement history of the Knidos fault, in the Western Turkey. Although this method can cause breakthrough to the recent studies in earth science, there are plenty of limitations and uncertainties to deal with. The important factors are latitude and air pressure (elevation) scaling factors for a constant geomagnetic field, shielding resulting from the specific geometry of active normal faults, effects of the chemical composition of the colluvial wedge, effects of denudation of the scarp surface and snow cover effects on scarp shielding. Through the modelling of the cosmogenic ^{36}Cl nuclides, it can be understood that Mezarlık Fault might be post-glacial as a result of previous studies implied in the similar fault scarps in the Mediterranean. As oppose to all of these limitations, it has been tried to understand impacts of these factors on the target fault by using recent numerical models. I have set out to obtain accurate conclusion through correlate and compare the result with synthetic profiles and previous studies as much as possible. The slip histories modelled via concentrations of 36Cl indicate that at least three or more events occurred on the Mezarlık fault within the past 20 kyr; over 10 meters of displacement took place between early Holocene and late Pleistocene. This study was conducted with the Decision of the Council of Ministers with No. 2013/5387 on the date 30.09.2013 and was done with the permission of Knidos Presidency of excavation in accordance with the scope of Knidos Excavation and Research carried out on behalf of Selçuk University and Ministry of Culture and Tourism. This study was supported by the TÜBİTAK (Project No: 113Y436).

KNİDOS FAY ZONU'NUN DEPREM GEÇMİŞİNİ KLOR-36 YÜZEY YAŞ TAYİNİ YÖNTEMİYLE MODELLEME

ÖZET

Bu çalışmanın amacı kozmojenik ^{36}Cl izotopu yaş tayini metodu aracılığıyla Knidos fayının deprem tekrarlama aralığını ve bu depremlerde meydana gelen atımları hesaplamak ve nihayetinde fayın geçmişteki sismik aktivitelerini tespit etmek. Çalışma alanındaki deprem tekrarlanma aralıkları, meydana kayma miktarları ve kayma hızları elde edilmesi, çalışma bölgesi için sismik tehlike değerlendirmelerinin daha sağlıklı yapılması imkân sağlar. Sismik tehlikelerin değerlendirilmesi sonucunda bölgede meydana gelebilecek olası depremlerin neden olabileceği hayati, beşeri, sosyal ve ekonomik kayıpların en aza indirilmesi için kritik yaklaşımlar sağlayabilir.

Depremler insanlık tarihi boyunca en beklenmedik ve yıkıcı doğal afetlerin başında gelmektedir. Bununla birlikte, depremler, sadece insan hayatını değil aynı zamanda kültürel ve tarihi miraslara telafi edilemeyecek hasarlar verebileceği gibi ekonomik, siyasi ve sosyolojik etkilerini de uzun yıllar boyunca hissettirebilir. Bilhassa, 1999 yılında şahsen de tecrübe ettiğim Kuzey Anadolu Fayı'nın batısında 7,4 büyüklüğündeki İzmit Depremi(Kocaeli ya da Gölcük Depremleri olarakta bilinen) ve 7,2 büyüklüğündeki Düzce depremi, bu hususta unutulmayacak tecrübeler yaşatmış, ayrıca depremlerin sonuçlarının nelere yol açabileceği hususunda çok kritik farkındalıklar yaratmıştır.

Tarihsel dönemlerde meydana gelen büyük depremler Ege ve Akdeniz'de şehirlerin yıkılmasına (Santorini, Efes, Antakya), büyük can kayıplarına ve uygarlıkların (Girit) ortadan kalkmasına neden olmuştur. Knidos, bu antik kentlerden biri olup, ülkemizin güneybatı ucunda bulunan Datça Yarımadası'nın en batısında yer almaktadır. Bu antik liman kentinin yaklaşık üç bin yıllık bir geçmişi bulunmaktadır. Bu liman kenti doğu yamaçlarında bir duvar gibi yükselen Knidos Fayı'nın dikliklerinin hemen önünde kurulmuştur. Bu nedenle arkeolojik dönemde fayda meydana gelmiş büyük depremlerin fiziksel kanıtlarını antik kent içinde görme şansı bulunmaktadır. Keza yapılan jeo-arkeolojik çalışmalar kentin içinde yer alan tapınak ve sütun gibi yapıların bu fay tarafından kesildiğini ya da yıkıldığını göstermektedir. Son yıllarda gerçekleştirilen jeolojik ve arkeolojik çalışmalar bölgede en az iki büyük sismik olayın meydana geldiğini işaret etmektedir. Bu çalışmalarda, ilk sismik olayın M.Ö. 2 – 3 yüzyıllar arasında, Afrodit Tapınağı ve Demeter Tapınağının yıkılmasına neden olduğu; ikinci olayın ise Yuvarlak Tapınak ve Demeter Tapınağı'nın yer değiştirmesine neden olduğu bildirilmektedir. Bu bilgiler ışığında hareketle, Knidos Fayı Zonu'nda meydana gelen kayma oranını ve deprem tekrarlama aralığı hakkında bilgi edinmek için 36Cl yüzey yaşlandırma yöntemini uyguladı.

Fay dikliklerindeki kozmik izotopların derişimlerinin modellenmesi, bu yüzeye etki eden tektonik ve yüzey süreçlerinin etkilerini anlamamıza yardımcı olabilir. Yüzey yaş tayini yöntemi, kozmik ışınlara maruz kalan fay düzleminde üretilen ender

kozmik nüklitlerin miktarının ölçülmesi esasına dayanır. Galaktik kaynaklı ve Güneş'te meydana gelen radyo aktif ışınım kaynaklı birincil kozmik ışınlar, genellikle protonlardan oluşmaktadır. Birincil kozmik ışınlar olarak adlandırılan bu parçacıklar, çok yüksek enerjiye sahiplerdir. Bu ışınlar, atmosferle çarpıştıklarında atmosferdeki elementlerle etkileşime girerek ikincil kozmik ışınlara dönüşürler. İkincil kozmik ışınlara dönüşen bu parçacıklar yeryüzüne ulaşır ve kayaçlarla etkileşime girerler. Bu etkileşim sonucu kayaçların yeryüzüne yakın yerlerinde, ağırlıklı olarak yaklaşık 2 ile 3 metrelik bölümlerde, değişik reaksiyonlar neticesinde nadir izotopları oluştururlar. Bu izotoplar kozmojenik izotoplar olarak adlandırılır. Özellikle kireç taşının kimyasal yapısında bulunan, kalsiyum (40Ca), potasyum, (39K) ve klor (35Cl) gibi elementlerin ikincil kozmik ışınlarlar etkileşimleri neticesinde kozmojenik Klor-36 (36Cl) izotopu oluşur. Bu izotopun oluşumunda yer alan kimyasal reaksiyonlar, yüksek enerjili spallasyon reaksiyonları, düşük enerjili nötron reaksiyonları(termal ve epitermal) ve müon reaksiyonları olarak sıralanabilir. Spallasyon reaksiyonları genellikle yüzeye yakın yerlerde baskın olmakla birlikte nüfus derinliğinin az olmasından dolayı etkilerini derinlikle üstel olarak kaybederler. Tepkimeye girme eğilimleri düşük olan müonların ise nüfuz derinliği daha yüksektir. Bu nedenle derinlikle gerçekleşen kozmik izotop üretimlerinden müon parçacıklarının neden olduğu reaksiyonlar yer alır.

Yüzey yaşlandırma yönteminin, sağlıklı bir şekilde uygulamaya geçirmek amacıyla, arazide çalışmaları gerçekleştirildi. Yapılan arazi çalışmalarında örneklemeye yapmaya elverişli ve amaca uygun fay diklikleri tespit edildi. Örnekleme aşaması çok önemli olduğundan örnek toplanacak fay dikliğinin belirli özel niteliklere sahip olması gerekmektedir. Hedeflenen fay dikliğinin alüvyal yelpazelerden, antropojenik etkilerden, dereler ve akarsu vadilerinden kesinlikle etkilenmemiş ya da en az etkilenmiş bir yapıya sahip olması gerekmektedir. Hedef fay dikliği tespit edildikten sonra örnekleme işlemi için gerekli hazırlıklara geçildi. Yapılan hazırlıklar, iş güvenliğinin en üst seviyede olması gerektirmektedir. Örnekleme işlemine geçilmeden evvel bu sürece dâhil olacak, ekibin yanında bulundurması gereken donanımlar: 1) Koruyucu kask, 2) Gözleri toz ve taş sekmelerinden korumak için emniyet gözlüğü, 3) Ağız, burun ve dişleri korumak için plastik yüz maskesi, 4) Solunum sistemini korumak için özel koruyucu maske, 5) Kulakları aşırı gürültüden korumak için kulaklıklar, 6) Fosforlu iş ceketi, 7) Ellerin güvenliği için koruyu iş eldivenleri ve son olarak 8) İlk yardım çantası. Örnekleme çalışması, son derece ciddi ve zaman alan bir işlem olması nedeniyle, yukarda sayılan temel donanım eksikliği durumunda işlem başlatılmamalıdır. Örnekleme çalışmasının gerçekleştirileceği fay dikliği, yaklaşık ~15m yüksekliğinde olması nedeniyle, tırmanış için profesyonel destek alınması gerekmektedir. Tırmanış için profesyonel destek alınmalıdır. Bu süreç boyunca çalışma ekibinde, ekibimsimizde her zaman süreç başında bulunan profesyonel bir dağcı çalışma arkadaşımız mevcut bulundu. Toplanan örneklerin taşınma sırasında dağılmamaları ve muhafaza edilmeleri amacıyla plastik folyolara sarılıp, özen bir şekilde silinmez kalemler aracılığıyla sırayla isimlendirildi. Örnekler fiziksel özellikleri tespiti ve gerekli kimyasal işlemlerden geçirilmek üzere Fatih Ünversitesi'ndeki Kozmo-Lab'a nakledildi. Kimyasal işlemlere başlamadan evvel, örneklerin ağırlık, yoğunluk ve ebatlarının ölçümleri yapıldı. Bu işlemlerden sonra örneklerin kimyasal işlemlere hazır ve uygun hale gelmesi için her bir örnek için ayrı ayrı kırma, öğütme ve eleme işlemlerinden geçirildi. Kimyasal işlemleri tamamlanan örnekler,Fransa'da bulunan CEREGE laboratuvarında Hızlandırılmış Kütle Spektrometresi (AMS) ölçümleri için gönderilmiştir.

Yaklaşık 15 metre yüksekliğindeki fay dikliğinden alınan, 128 örnekten ölçülen 36Cl derişiminin modellenmesi, Türkiye'nin batısında bulunan Antik Knidos Kenti'nde bulunan faylardan, Mezarlık Fayı'nın geçmişte meydana gelen sismik olaylar neticesi meydana gelen kayma miktarlarını ve bu olayların tarihlerini belirli ölçüler dâhilinde hesaplamaya olanak sağlamaktadır. Kozmik izotopların üretim oranı, negatife muon yaklaşması, düşük enerjili nötron yakalanması ve spallasyon reaksiyonlara bağlıdır. Bu yöntem her ne kadar yer bilimlerinde büyük bir ilerleme hususunda katkıda bulunmuş olsa da, model üzerinde düzeltilmesi gereken belirsizlikler ve kısıtlamalar mevcut. Bu etkenler, sabit yer manyetik alanı değeri altında enlem ve yükseklik ölçeklenmesi, belirli bir geometriye sahip aktif fayın perdelenmeye göre ölçüm düzeltmesi, kolüvyon kimyasal bileşenlerine göre ölçüm düzeltmesi, alansal erozyon etkilerine göre ölçüm düzeltmesi ve kar örtüsü etkisi altındaki ölçüm düzeltmesi şeklinde sıranabilir. Önceki çalışmalarda, Akdeniz bölgesinde bulunan benzer fay dikliklerinin buzul dönemi sonrası olabileceğini fikrinin Knidos Fay Zonu ile uyumlu olup olmayacağı bu yöntem aracılığıyla tespit edilebilir. Modelleme, büyük kayma olaylarını tanımlamaya olanak sağlasa da, bu olayların bir ya da birden fazla olay olup olmadığını ayırt edememektedir. Bu hususta meydana gelen olayların irdelenmesi açısından tespit edilen olaylar, büyük sismik olaylar veya olaylar serisi şeklinde değerlendirilmelidir. Kozmik izotop derişimlerinin modellenmesi sonucunda elde edilen en uyumlu model en az üç büyük depremi işaret etmektedir. Bu olayların meydana geldiği tarihler geçmişten günümüze 18.7, 15.0 ve 10.8 bin yıl olarak belirlenmiştir.

Bu çalışma, 30.09.2013 tarih ve 2013/5387 sayılı Bakanlar Kurulu Kararı ile Kültür ve Turizm Bakanlığı ve Selçuk Üniversitesi adına sürdürülen Knidos Kazı ve Araştırmaları kapsamında ve Knidos Kazı Başkanlığı'nın izni ile yapılmıştır. Bu çalışma TÜBİTAK tarafından desteklenmektedir (Proje No: 113Y436).

1. INTRODUCTION

Owing to lack of instrumental record history of earthquakes, different methods can be feasible to provide information seismic history of active faults. One of these approaches is digging a paleoseismic trench across a fault, as it is well known that gives information about such as few past major earthquakes and occasionally displacements. However, it is not always easy to overcome where datable material is not existed within the trenched deposits (Carcaillet et al., 2008). On the other hand, there is another method as known in situ cosmogenic ^{36}Cl surface exposure dating can be preferable when facing paleoseismological obstacles, instead.

In situ cosmogenic ^{36}Cl surface exposure dating of limestone fault scarp is based on dating of multiple samples that can be taken on a scarp of a limestone fault providing important information about seismic history. Moreover, through this method, it may be calculated timing and displacements of earthquakes. (Zreda and Noller, 1998; Mitchell et al., 2001; Benedetti et al., 2002, 2003, 2013; Palumbo et al., 2004; Schlagenhauf et al., 2010, 2011). Using cosmic-ray surface exposure dating of a well-preserved limestone fault scarp facilitates us to attain information, which reveals a seismic history of faulting events and identifies timing and their recurrence interval of major earthquakes and slip rates of the Knidos Fault Zone.

Despite the fact that ^{36}Cl dating provides very important information about seismic history of faults, there are uncertainties such as topographic shielding, colluvial wedge density, denudation to be dealt with which help us make the inferences more accurate (Gosse and Phillips 2001; Schimmelpfennig et al., 2009; Schlagenhauf et al., 2010). Previous studies show that especially all through the Mediterranean Basin, bedrock faults have preserved their scarps (Reicherter et al., 2014) and those are the Hebgen Lake fault in Montana United State of America (Zreda and Noller, 1998), in the Northern Israel Nahef East fault, (Mitchell et al., 2001) in the Southern Greece, Sparta and Kaparelli fault (Benedetti et al., 2002, 2003) and in central Magnola-Velino fault (Palumbo et al., 2004; Schlagenhauf et al., 2010, 2011). The latest numerical analysis which is developed by Schlagenhauf et al. in 2010 were used here

not only provides deduction of slip rates, reoccurrence interval of earthquakes but also helps to remove some level of uncertainties (Schlagenhauf et al., 2010). This method is a powerful tool to reconstruct seismic history of normal faults and critical to understand regional seismic hazard. It is focused on one of the most prominent fault scarps (hereinafter mezarlik fault) stretching along the antique Knidos city. In the light of these developments, especially numerical models, it has been applied in situ ^{36}Cl surface exposure dating of the Mezarlık fault scarp, which give us chance to make inference of the seismic history of active fault. Thus, I applied recently developed models to the study site in order to assess the earthquake slip history of the cumulative scarp of the Mezarlık fault through determining concentration rate of cosmic ^{36}Cl isotopes (Schimmelpfennig et al. 2009, 2011; Schlagenhauf et al., 2010). In order to get information about seismic hazards, fault parameters such as moment magnitude, rupture length, slip rate and recurrence are very important in active tectonic studies. Magnitudes of earthquakes are one of the most important factor in seismic hazard analysis. Through displacement data, moment magnitudes of earthquakes can be estimated using empirical equations (Wells and Coppersmith, 1994).

In the conclusion part, it will be touched upon important implication of in situ cosmogenic ^{36}Cl dating. At the end of all these analysis using this approach, we might able to decide which earthquakes or earthquakes clusters cause can highest slip rates, amount of displacement and reoccurrence interval of earthquakes. Concordantly, these values might be significant basis for anticipated ruptures along the active fault and furthermore, it may contribute seismic hazard assessment of the Knidos.

2. STUDY AREA

It is widely known that the Western Anatolia is one of the most seismically active and rapidly extending regions in the world. (Bozkurt, 2001). The Knidos Fault Zone is situated in ancient settlement ruins on the Datça Peninsula located in the SW Turkey.

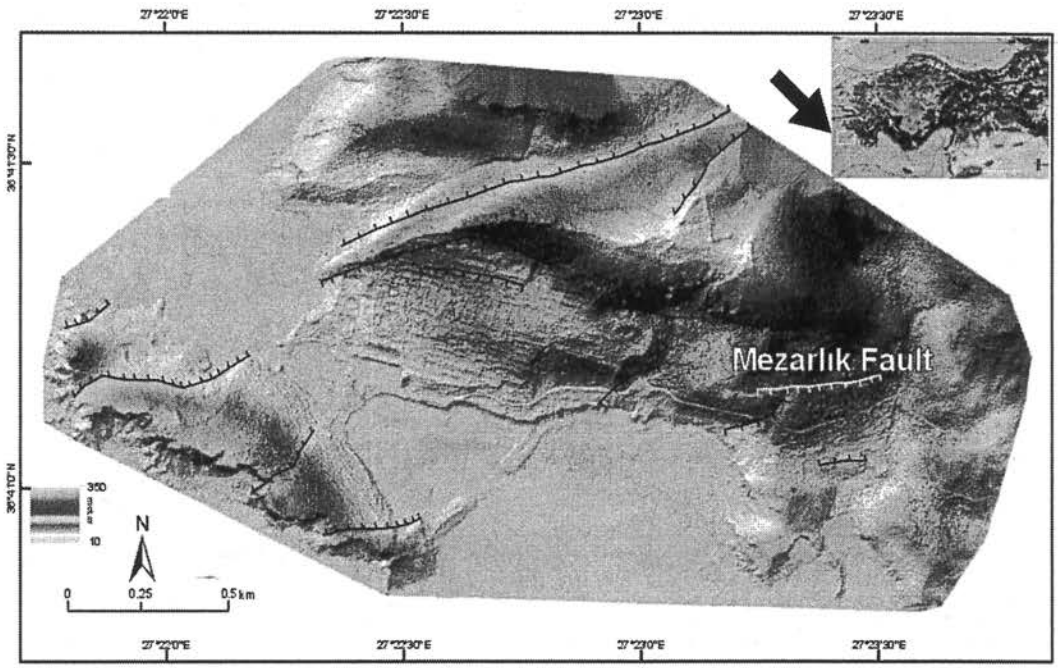

Figure 2.1: Active fault map of the Knidos Peninsula (modified after Altunel et al. 2003).

The Datça Peninsula defines southern boundary of both the Gulf of Gökova and the Western Anatolian Extensional Province. The seismic history of the Knidos Fault Zone is therefore may provide insights about fault activity covering millennial scale to Pleistocene scale in the Southern Aegean Region. Datça Peninsula was affected by earthquakes that occurred in Gulf of Gökova throughout historical and instrumental period (Table 2.1). The recent geological and archaeological evidences point out that this ancient site was affected by at least two crucial momentous seismic events (Altunel et al., 2001). The total length of the fault is 8 km eastwards and creates a very distinct mountain front. The fault consist of two main segments, which are trending W-E direction (Figure 2.3). Two distinct faults that located in the study area

called the Demeter fault and the Mezarlık fault. It has been chosen to aim at the Mezarlık segment because of that it has well preserved and absence of any sort of anthropogenic effect and denudation and most prominent fault scarp stretching along the antique Knidos city.

Table 2.1: Destructive historical earthquakes of the region (Dirik, 2007).

Date	Latitude	Longitude	Location	Itensity
BC 222	36.5	28	Rhodes (Tsunami)	X
BC 185	36	28	Rhodes	IX
155	36.3	28	Rhodes, Muğla,Fethiye	X
08.08.1304	36.5	27.5	Rhodes,Crete	X
03.10.1481	36	28	Rhodes, SW Anatolia(Tsunami)	IX
18.08.1493	36.75	27	Kos	IX
18.10.1843	36.25	27.5	Rhodes, Aegean Sea	IX
12.10.1856	36.25	28	Rhodes,Crete(Tsunami)	X
22.04.1863	36.5	28	Rhodes	IX
29.03.1885	37.2	27.2	Aegean Sea	IX

Knidos Fault Zone has a special place in terms of its archaeological and geological properties. The geoarcheological studies in this antique city indicate that presence of structures such as temples and walls cut off by Knidos Fault. These observations show that Knidos fault is active (Altunel et al., 2001; Dirik, 2007).

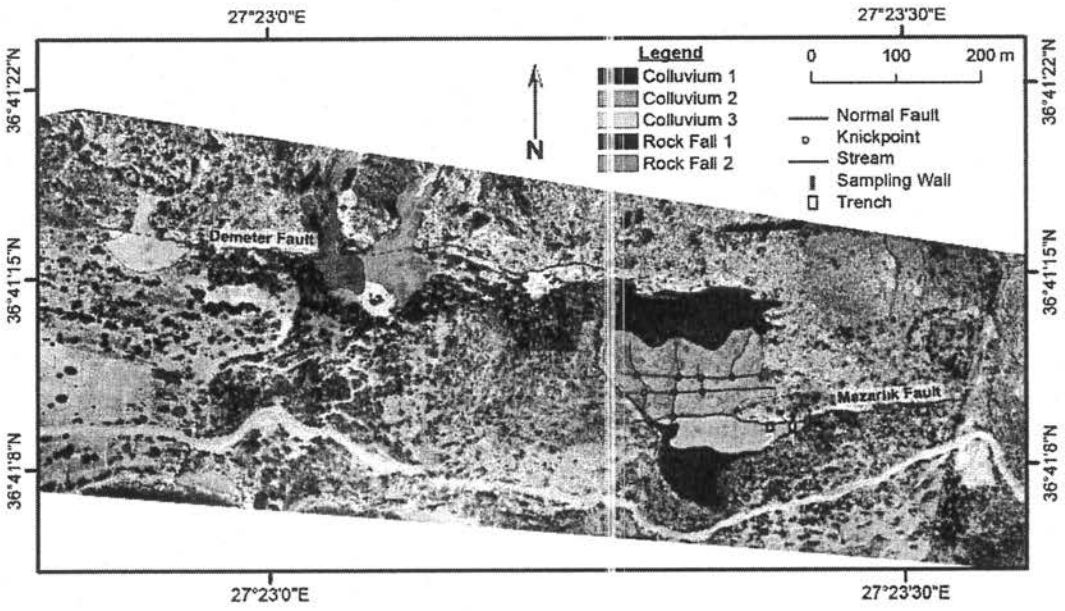

Figure 2.2: Geomorphic map of the target area.

As it is seen on the tectonic geomorphological map (Figure 2.2), it shows that there are three knickpoints the western part of the Mezarlık fault scarp and three different

colluvial phases. Those might be correlated with major slip events, which can form them. The Mezarlık fault scarp is almost 300 m long and ~15 m average high, where the fault scarp was developed in neritic limestone, which is Jura-Cretaceous age, which is very suitable for ^{36}Cl surface exposure dating.

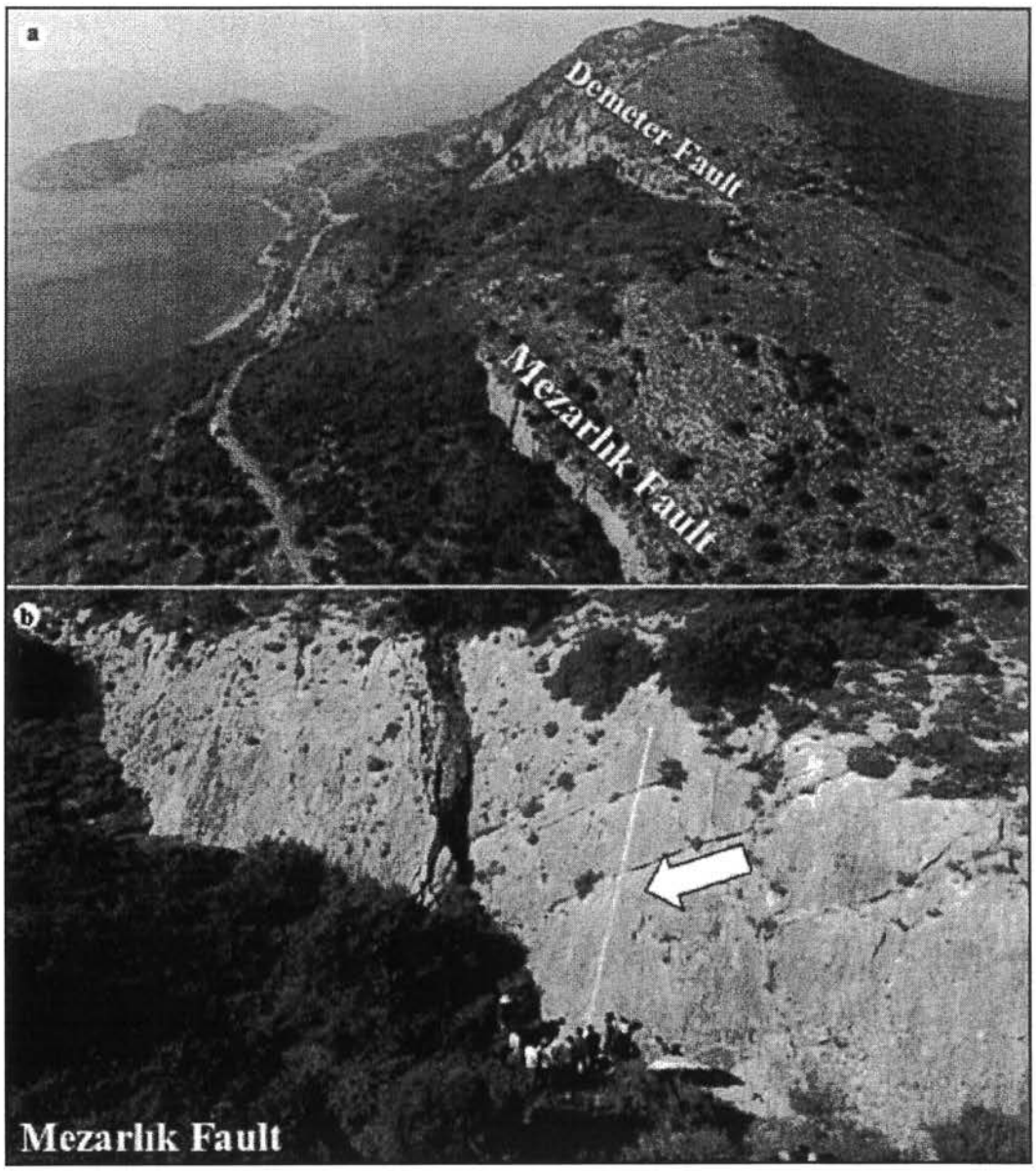

Figure 2.3: a) Oblique view of Demeter and Mezarlık fault scarps (from SE to NW). b) Thin white line indicates sampled part of scarp.

2.1 Sampling

Sampling was performed on the Mezarlık fault's scarp from top to base along its slip direction. 128 continuous samples were collected which were 20-cm wide and 10-cm long and 3-cm thick. Besides these, a ~2 meters deep trench was opened at the base of the scarp for paleo-seismological research. It is crucial to choose sampling site due

to principle of method, complexity of chemical analysis and degradation effects on fault scarp. Thus, sampling site was chosen to avoid those kind of problems such as rivers, gullies, intense colluvial deposits and the preservation of scarp. Furthermore, sampling was carried out amount of cumulative slips as high as possible on the fault.

2.2 Personal Protection

Before starting to perform anything on the field, there are lots of vital safety equipment that must be provided along with first aid kits.

While trying to cut rocks on the fault scarp surface, there will be great deal of dust that block one's vision and respiration. For anyone's safety, some equipment such as hardhat, goggles, gloves, dust respirators, ear defenders, and kneepads are top priority. A hard hat to prevent any sort of accidents such as head injuries ; goggles for eye protection from dust and chippings; plastic face mask or dusk mask to protect face, nose, month and teeth. Dust mask to avoid from breathing in dangerous particles; ear defenders that can help blocking angle grinder noise as power tools make so much noise. Safety vests specially the one, which has reflector features. Work gloves that important for any operation in the fieldwork. Not only the one who works for sampling but also anyone who is around the fault scarp should wear safety equipment. After finishing those preparations, equipment can be set up.

2.3 Climbing

The climbing equipment was used for building anchors steel carabiners along with bolt and bolt hanger and dyneema slings for equalizing the anchors. In order to ascend jumar and chest jumar, Peltz Ascension for descending Petlz I'D was used which is self-breaking descender to rescue with anti-panic function. As for personal safety helmet, climbing harness, carabiners, clings and prusik cords. At first, any suitable anchors were checked on upper part of the fault scarp. The worst case scenario would have been bolting if we had not found any convenient place for anchors, but trees were found as a natural safety point and we used the tree as an anchor to avoid harming the natural environment. In order to make sure of safety of the one who uses angle grinder, two (2) ropes were used for permanent lines. One of the ropes was used for descending by ID, the other one was used for backup through

prusik knot. Jumar and chest jumar were used in order to ascend on the rope. The target scarp was chosen whether it fit properly circumstances as stated above, rectangle wood plaque was used for drawing two straight-lines to enclose the certain sampling parts of the scarps after those preparations had been completed sampling was performed (Figure 2.4).

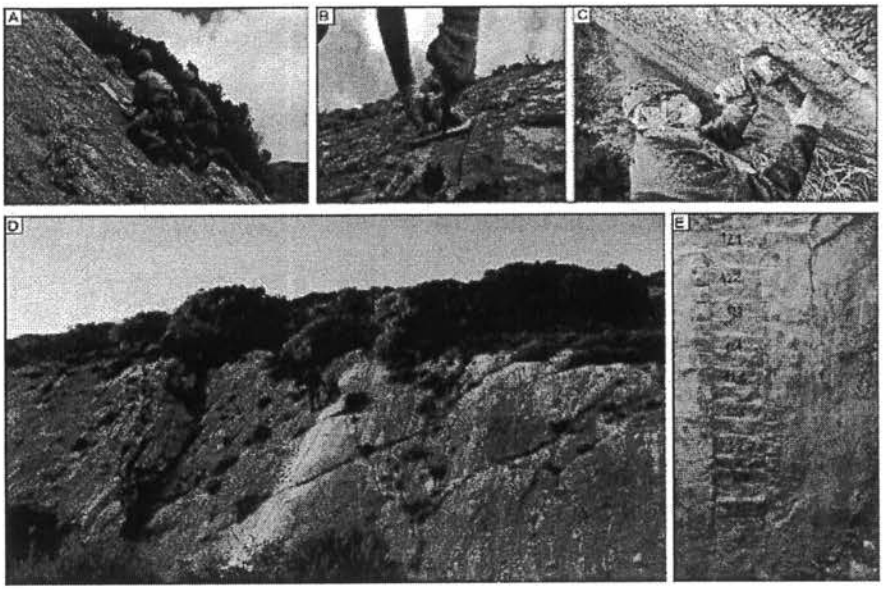

Figure 2.4: Field photograph of sampling processes.

2.4 Equipment Preparation

Sampling on fault scarps is both challenging and dangerous and it is also a time consuming process, depending number of your samples. As generators make really much noise while they are working, it is preferred to set it up away from sampling location as much as possible. In addition to that, using power strip, which has very long cables, can help to solve this problem to some extent. It was used an "angle grinder" (Figure 2.4) which is a handheld tool for cutting samples on the fault scarp. However, those tools are extremely powerful and dangerous; for this reason, it might cause accidents if it is used carelessly. On account of that, before operating anything, one must get training and instruction manual should be read and carefully followed especially for electrical power tools.

3. METHODOLOGY

In situ ^{36}Cl surface exposure dating is based on cause of the production of rare nuclides in exposed rocks, which interacts with secondary cosmic rays (Gosse and Phillips, 2001). The reason of production in situ cosmogenic ^{36}Cl in the rocks that is muons and neutrons interact with target elements in limestone and those are ^{39}K, ^{40}Ca, and ^{35}Cl whereas almost the earth's crust surface and a few meters top of rocks. By the aid of calculation of cosmogenic ^{36}Cl concentration in limestone, we can make estimation of slip rates, timing of faulting events and recurrence intervals of earthquake (Zreda and Noller, 1998; Gosse and Phillips, 2001; Mitchell et al., 2001; Benedetti et al., 2002, 2003, 2013; Palumbo et al., 2004; Schlagenhauf et al., 2010, 2011). Although exposure history methods provide important information of paleo-seismicity, correction of altitudinal scaling and the temporal variations in production should be done (Gosse and Phillips, 2001). In absence of all of the shielding effect on fault scarp, it can contribute to the ^{36}Cl concentration and so, we come up with a simple scenario of overall process.

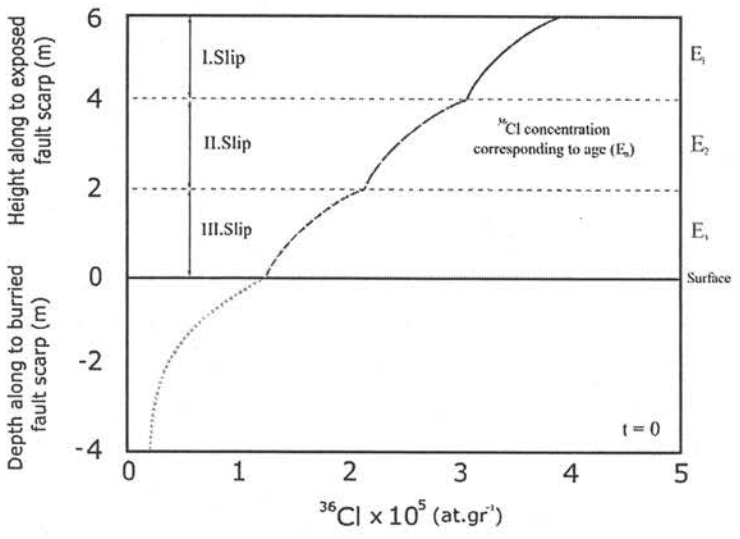

Figure 3.1: Synthetic profile of and concentration of ^{36}Cl.

The production rate of cosmogenic ^{36}Cl isotopes decrease exponentially along with depth due to substantial amount of cosmogenic nuclides are found closest part of rock surface (Gosse and Phillips, 2001). As it is seen on Figure 3.1 each earthquake

causes exhumation of new portion of the fault scarp above the surface and synthetic profiles that is modelled for three successive faulting events. However, when we study on real date beyond these synthetic profiles and data, the results will be more complicated. Through all of these analyses, various scarp versus ^{36}Cl concentration should be tested. On the purpose of testing different scenarios, couple of statistical methods can be used. One of these methods called root mean square (RMS) is to help determining the best-fit scenario between data and the model (Palumbo et.al, 2004).

$$RMS = \sqrt{\sum_n \left(^{36}Cl_{measured} - {}^{36}Cl_{model}\right)^2 / n} \quad (3.1)$$

It is one of the most preferred approach to test distribution of dataset. The principal pointer that one may utilize is the weighted root mean square (RMSw) which permits evaluating the fit in the middle of displayed and measured fixations while considering the instabilities on the estimations.

$$RMSw = \sqrt{\sum_{i=1}^{n} \left[\left(\frac{^{36}Cl_{measured} - {}^{36}Cl_{model}}{i\sigma^{36}Cl_{measured}}\right)^2\right] / n} \quad (3.2)$$

At that point ascertaining for every best model situation Akaike Information Criterion concluded the best situation (Palumbo et.al, 2004). The norm incorporates not only just the goodness-of-fit between the model and the information additionally the quantity of parameters incorporated into the model, along n the number of data points and p the number of independent parameters that correlates to the number of events:

$$AIC = nlog\left[\sum_n \left(^{36}Cl_{measured} - {}^{36}Cl_{model}\right)^2 / n\right] + 2p \quad (3.3)$$

In this formula $^{36}Cl_{measured}$ is the qualified AMS combination in ^{36}Cl, $^{36}Cl_{model}$ is the modelled combination in ^{36}Cl, σ ^{36}Cl qualified is the ambiguity on the AMS measured ^{36}Cl combination, and n is the quantity of estimation. Furthermore, it was additionally used another analysis of the Akaike Information Criterion (Akaike, 1974). Where the parameters are characterized recently. At the point when the proportion of the information number n to the quantity of free parameters k is little ($\leq$40, Burnham and Anderson 2002), a more refined rendition of the AIC model, named AICc, must be applied:

$$AICc = n\,log\left[\sum_n\left({}^{36}Cl_{measured} - {}^{36}Cl_{model}\right)^2/n\right] + \frac{2kn}{n-k-1} \quad (3.4)$$

After the combination of two equations (3.3) is produced. In all of these models, the most strong is the one having the least AICc rate. Some other models are then positioned by contrast between its own AICc esteem and this rate. Models with $0 \leq 2$ are sensibly very much upheld by the statistics, models with $3 \leq 6$ are less upheld by the information yet still probable, while models with $10 \leq$ are not upheld by the statistics and ought to be disposed (Burnham and Anderson 2002, Schlagenhauf et al., 2010). Major activity of the fault particularly Holocene and Pleistocene can be kept tracking using distribution of in situ ^{36}Cl concentration and scarp height via scatter plot. Without effects of denudation, ^{36}Cl concentration of a particular cosmic nuclide can be calculated function of time and depth, as

$$dN(z,t)/dt = P(z,t) - \lambda \times N(z,t) \quad (3.5)$$

Where dN/dt is rate of change in time, λ is the decay constant, P is the isotope production rate, P is the isotope rate, t is rock exposure time and z represents depth. The decay constant specific for each element for ^{36}Cl decay constant: λ_{36} = 2.303 x 10^{-6}. a^{-1}. In absence of all the shielding effects on fault scarp which can contribute to the ^{36}Cl concentration, we come up with a simple scenario of overall process. As a consequence of temporal variation of cosmic ray flux and evolution of geomorphic features through time, then one considers those effect and then production rate can calculate as function of all of these parameters below equation (3.5).

$$P_{total} = S_{el,\mu}F_\mu Q_\mu P_\mu(z) + S_{el,s}F_s Q_s P_s(z) + S_{el,s}F_n[Q_{eth}P_{eth}(z) + Q_{th}P_{th}(z)] \quad (3.6)$$

Total production rate (P_{total}) is sum up of different type of reactions. S, F and Q are scaling factors respectively along with those subscripts refer to: El, for elevation and latitude; s for spallation reactions of Ca, K, Ti and Fe; μ for direct capture of slow negative muons (^{40}Ca and ^{39}K); eth for capture of specific epithermal neutron (^{35}Cl); th for capture of specific thermal neutron (^{35}Cl); rad, for radiogenic production; n, for capture of all types of low-energy neutrons.

$S_{el,s}$ is summed effect of latitude and elevations for spallation; $S_{el,n}$ summed effect of latitude and elevations for thermal and epithermal neutrons; S_μ summed effect of latitude and elevations for slow negative muons. Due to time dependency of magnetism that might vary in time, temporal variations of the geomagnetic field are

included. P_x is the sample-specific ^{36}Cl production rate resulting from reaction x, as a function of sample chemical composition. P_s the sample specific ^{36}Cl production rate resulting from spallation (Ca, K, Ti, Fe etc.); P_{eth} the sample specific ^{36}Cl production rate resulting from capture of specific epithermal neutron; P_{th} the sample specific ^{36}Cl production rate resulting from capture of specific thermal neutron; P_μ the sample specific ^{36}Cl production rate resulting from capture of slow negative muons P_{rad}, the sample specific ^{36}Cl production rate resulting from radiogenic production. Q_x is the sample thickness integration factor for the reaction x, required from the production rate being calculated at mass depth z in g cm^{-2}.Q is thickness integration factor for spallation; Q_{eth} thickness integration factor for epithermal neutron; Q_{th} thickness integration factor for thermal neutron; Q_μ thickness integration factor for slow negative muons. F_x is a scaling factor of sum up all the correction for as topographic shielding, snow shielding and geometry. F_s shielding factor for spallation; F_n shielding factor for epithermal neutron + thermal neutrons; F_μ, shielding factor for slow negative muons ; $0 < Fx \leq 1$; $Fx = 1$ is no shielding.

3.1 Primary Cosmic Rays

The primary cosmic rays that are responsible for production of cosmogenic isotopes primarily come from outside the solar system and within Milky Way Galaxy. They majorly consist of high-energy radiation, mainly protons, when these particles strike upper atmosphere causing disintegrations of different particles when strike to the atmosphere of the Earth (Gosse and Phillips, 2001).

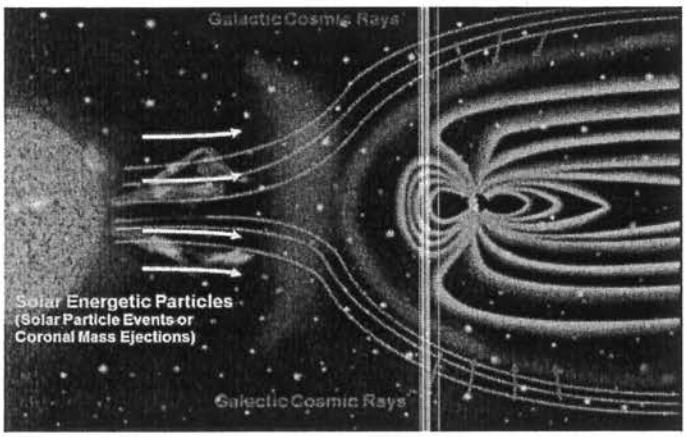

Figure 3.2: An illustration of origin of the galactic cosmic radiations (Source: NASA).

The cosmic rays that are responsible for production of cosmogenic isotopes, majorly consist of high-energy radiation, mainly protons, primarily comes from outside the solar system and within Milky Way Galaxy. When these high-energy nucleons enter atmosphere of the earth, it causes extensive cascade of secondary particles, which is called secondary cosmic rays. These particles mentioned as "terrestrial in situ cosmogenic nuclides" in order to imply differences between nuclides produced in the atmosphere and produced within minerals and rocks close to Earth's surface (^{3}He, ^{10}Be, ^{21}Ne, ^{26}Al, ^{36}Cl). The important note for processes that is all of the ^{36}Cl production rates and calculations based on the available literature (Stone et al. 1996, 1998, 2000; Gosse and Phillips 2001; Schimmelpfennig et al. 2009, 2011; Schlagenhauf et.al, 2010, 2011; Marrero, 2012).

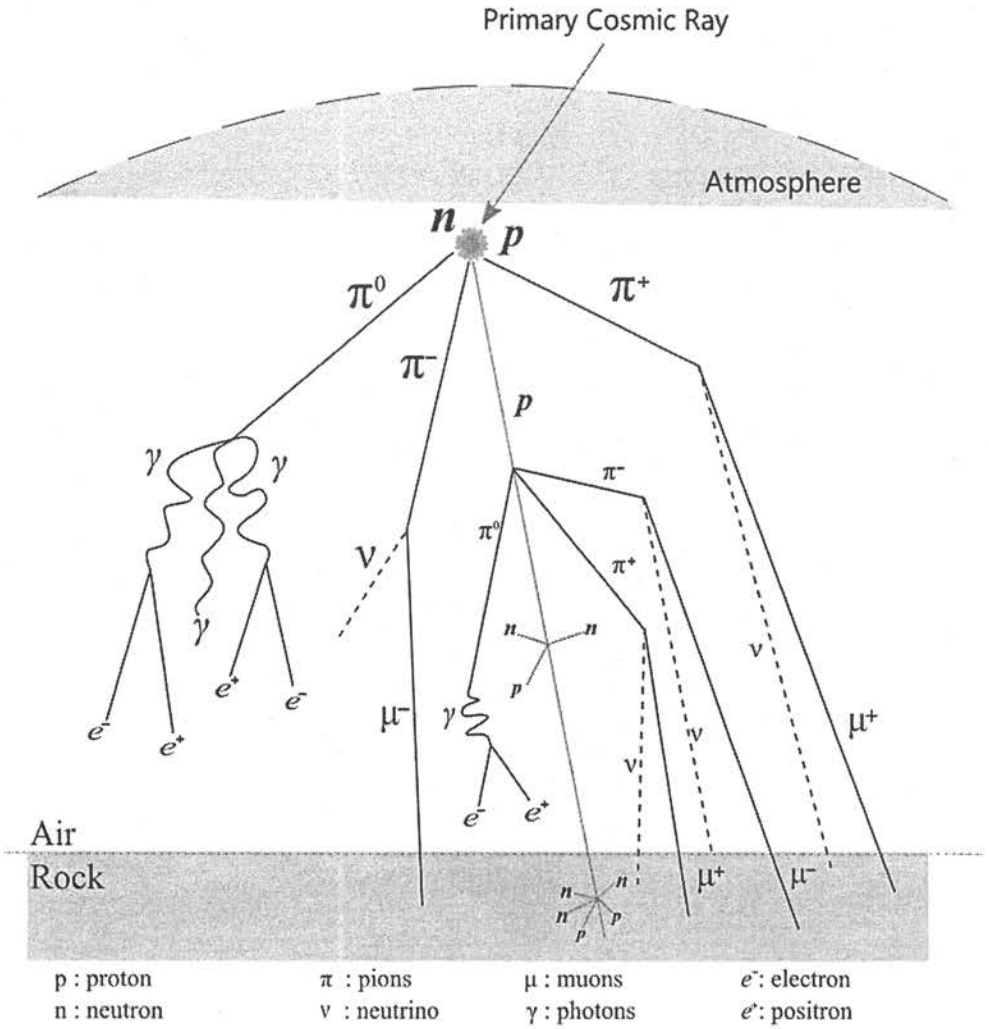

Figure 3.3: Path of the cosmic rays and those particles (Simplified after Gosse and Phillips, 2001).

Moreover, all of the formulas, equations and descriptions were taken exactly from a certain scientific publications (Gosse and Phillips 2001; Schimmelpfennig et al.

2009, 2011; Schlagenhauf et.al, 2010). Flux intensity of cosmic radiation comes from atmosphere in the direction given the angle of inclination θ and the azimuth ϕ given equation (3.6)

$$I(\theta, \phi) = I_0 \sin^m \theta \tag{3.7}$$

Both for $\theta > 0$ and for $\theta < 0$, $I(\theta, \phi) = I_0$. When exposed sample is not shielded, then it receives max possible flux then flux will be calculated as below:

$$\Phi_{max} = \int_0^{2\pi} \int_0^{\frac{\pi}{2}} I_0 sin^m \theta \ cos\theta \ d\theta d\phi = \frac{2\pi I_0}{m+1} \tag{3.8}$$

In case of topographic shielding, amount of cosmic radiation flux reduces by scaling factor $S = \Phi / \Phi_{max}$ next to the geology is depicted have a relationship between its vertical angle $\theta_{topo.}$

3.2 Secondary Cosmic Rays

The method that has been used in this study is based on the fact that the interaction of cosmic rays with the rocks exposed at the Earth's surface produces specific cosmogenic isotopes within these rocks (Gosse and Phillips, 2001). As limestone is geologically abundant and mostly consists of calcite minerals, cosmogenic ^{36}Cl production rate from Ca spallation convenient for dating (Stone et al., 1996).

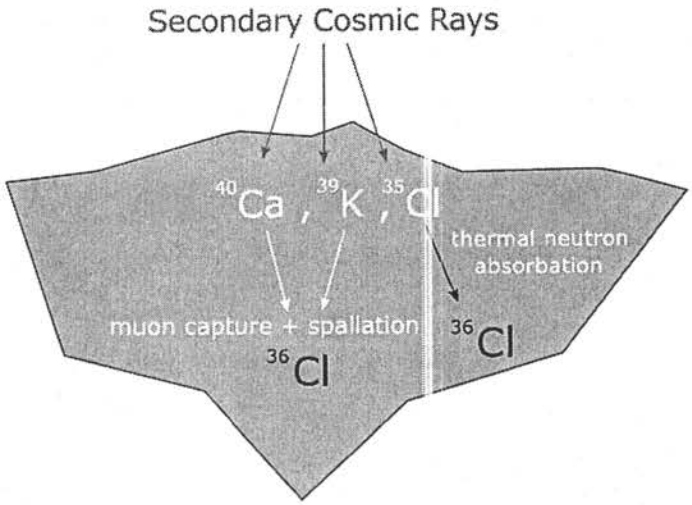

Figure 3.4: A simplified representation of the in situ ^{36}Cl isotopes production through interacting with target elements in limestone.

Limestones include the target elements that interact with secondary cosmic radiation which those are ^{39}K, ^{40}Ca, and ^{35}Cl. After exhumation of fault scarp, exposed to cosmic radiation, these elements take part in the production of ^{36}Cl as target

elements. Owing to the intensity flux of the cosmic ray, in situ ^{36}Cl can be produced by three main processes depending upon amount of energy of cosmic radiations (Figure 3.3). Moreover, cosmic ray flux intensity reduces along depth of limestone. There are three main processes which take place produce of cosmogenic ^{36}Cl isotopes (1): spallation which is a nuclear reaction result from collusion of target elements of rock Ca, K, Ti and Fe and secondary cosmic radiation (highly energetic neutrons), (2): capture of slow negative muons by ^{40}Ca and ^{39}K in that of muon can go through to greater depth of Earth thus production increases along penetration depth and (3): capturing of thermal and epithermal neutrons (or low-energy neutrons) by ^{35}Cl. Additionally, when samples have high U and Th concentrations, ^{35}Cl captures some of the low-energy neutrons generated during the decay of U and Th (non-cosmogenic) and these reactions cause production of cosmogenic ^{36}Cl as well (Schimmelpfennig et al., 2009, Schlagenhauf et al., 2010). Calibration of production rate is one of the crucial phases of calculation. Because of that, it has been taken account all of different type of reactions production rate while making calculations.

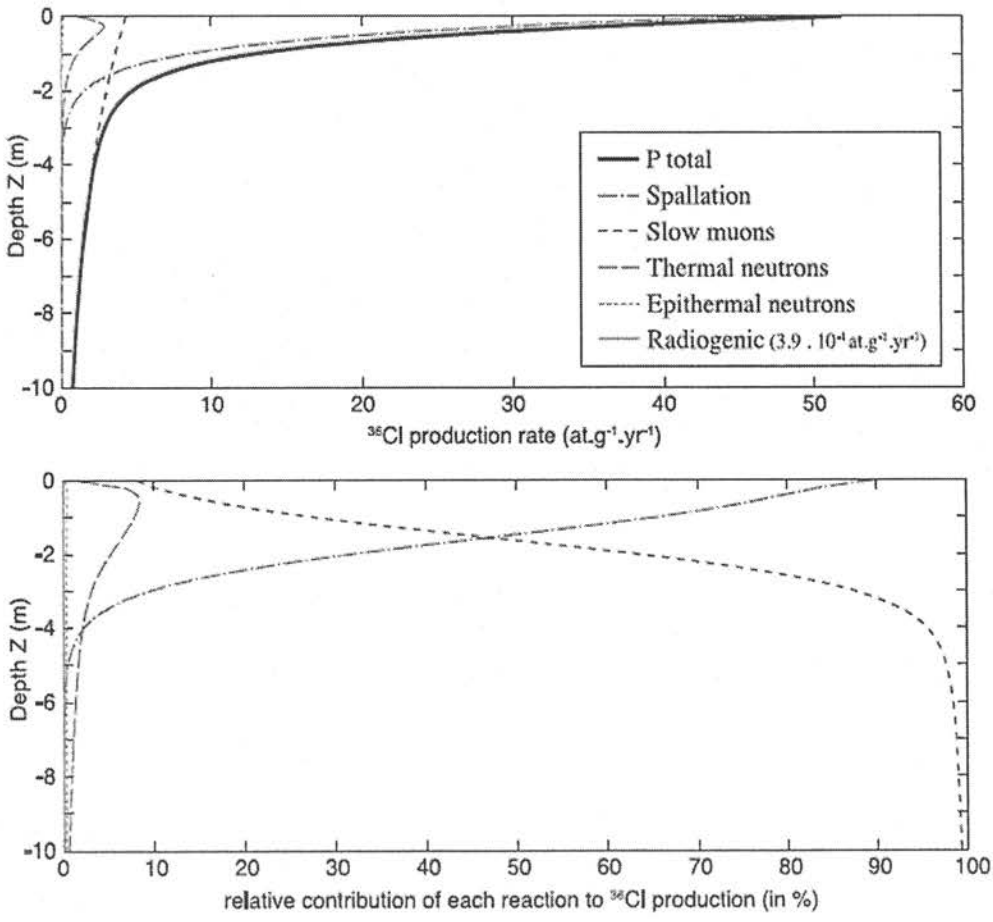

Figure 3.5: Contribution of the various cosmogenic source (From Schlagenhauf et.al, 2010).

3.3 Latitude and Altitude Scaling Factors

Dependency of the production rate of the ^{36}Cl isotope is relevant to two parameters, which are air pressure and geomagnetic field. The amount flux of cosmic ray shows varied response when it interacts with Earth's magnetic and atmosphere. Thus, the production rate of the ^{36}Cl isotope depends upon both the geomagnetic latitude and altitude of the study area. Even if we assume that Earth's magnetic field is constant through time, magnetic flux lines show differences from equator to poles. Deflection of cosmic radiation flux shows minimum value at the equator but it intensifies in along with latitudes (Schlagenhauf et al., 2010). In this model, it is assumed that both geomagnetic field and atmospheric pressure is constant through time. The scaling factor which has been mostly used in models for the purpose of considering the effects of latitude and elevation of neutrons ($S_{el,s}$) and muons, ($S_{el,\mu\_}$) and at the sea level high latitude (SLHL) these both values $S_{el,s} = 1$ and $S_{el,\mu\_} = 1$ as considered scaling factors (Stone, 2000; Schlagenhauf et al., 2010).

Spallation rate at latitude λ and elevation z (normalized to its value at 60° latitude and at standard sea level pressure):

$$S_{el,s}(P) = a + b + exp\left(-\frac{P}{150}\right) + cP + cP^2 + eP^3 \tag{3.9}$$

with a; b; c; d; e : scaling coefficients function of latitude from 0 to > 60° with a 10° step (see Stone, 2000), and P : Pressure (hPa) - (from Lal., 1991).

$$P(z) = P_s\, exp\left[\left(-\frac{g_o M}{R\xi}\right) ln T_s - \ln(T_s - \xi z\right] \tag{3.10}$$

Slow muon capture at latitude λ and elevation:

$$S_{el,\mu}(P) = M_{\lambda,1013.25}(\exp(1013.25 - P)/242) \tag{3.11}$$

with the attenuation length of muons in the air = 242, and $M_{\lambda,1013.25}$: scaling coefficients for latitudes from 0 to > 60° with a 10° step (see Stone, 2000).

3.4 Shielding Effects

In a good light, absence of topographic shielding, secondary cosmic radiation easily interacts with exposed fault scarps. However, the circumstances are not always that simple when we are in nature. It is a significant factor and must be taken into

consideration whether the sampling site surrounding high topography or not. If one encounters such a problem, the calculation of the production rate modifies against this effect. Normal fault geometry has three different dip parameters; these are the dip of colluvium α, the dip of fault scarp β and γ the dip of upper part of fault scarp (Figure 3.8). It is considered in this model that the fault scarp is semi-infinite plane. H refers to height of the scarp, α dip of colluvium, β the dip of scarp and γ the dip of the older fault section. A represents the exhumed samples receive cosmic radiation coming through the air and cosmic radiation passing through the rock; B represents the buried samples that only receive cosmic rays passing through the colluvium. The relationship between $\theta_{topo(\phi)}$ and ϕ depend upon azimuth (ϕ) given equation (3.16).

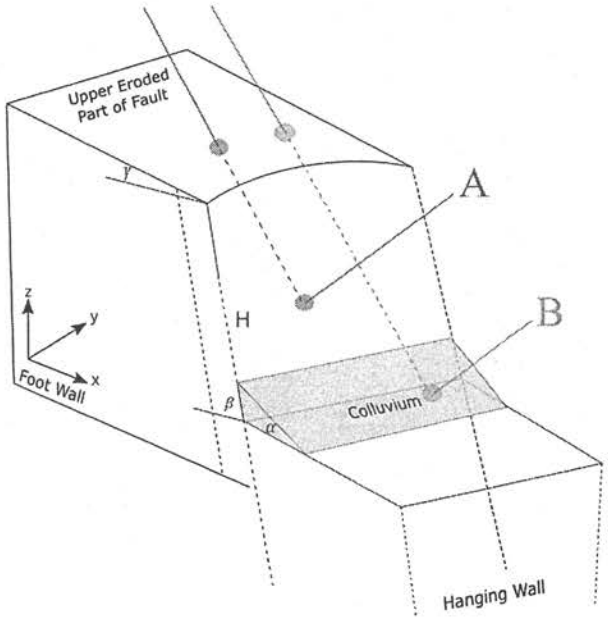

Figure 3.6: Representative illustration of expected fault geometry (Modified after Schlagenhauf et.al, 2010).

$$\theta_{topo(\phi)} = atan(tan\beta\, sin\phi),\ 0 \leq \phi \leq \pi \tag{3.12}$$

$$\theta_{topo(\phi)} = 0,\ \pi \leq \phi \leq 2\pi \tag{3.13}$$

The resulting shielding factor $S(\beta)$ is given as below

$$S(\beta) = \frac{1}{2} + \frac{m+1}{2\pi} \int_0^{2\pi} \int_{\text{atan}(tan\beta\, sin\phi)}^{\frac{\pi}{2}} sin^m\theta\, cos\theta\, d\theta d\phi \tag{3.14}$$

Measuring concentration of the shielded samples contain insignificant amount of ^{36}Cl due to less interaction of cosmic rays. The cosmic ray flux that from the direction of (θ, ϕ) at the sample will be attenuated by a factor exp $(-d/\lambda)$ where d is the distance travelled and λ is the true attenuation length. When the fault scarp height is

measured as H and the position of the sample on the scarp surface is measured by Z (positive upwards), then d is given by

$$d = \frac{(H-Z)\sin(\beta-\gamma)}{\sin\theta\cos\gamma-\cos\theta\sin\gamma\sin\phi} \quad (3.15)$$

The net contribution is as below

$$\Phi = \int_0^{\pi} \int_0^{\text{atan}(\tan\beta\sin\phi)} I_0\, e^{-\frac{d}{\lambda}} \sin^m\theta\cos\theta\, d\theta d\phi \quad (3.16)$$

The total flux received by the sample can then be calculated and leads to the following scaling factor $S_s(Z, H, \beta, \gamma)$ as below

$$S_s(Z,H,\beta,\gamma) = \frac{1}{2} + \frac{m+1}{2} \int_0^{\pi} \int_{\text{atan}(\tan\beta\sin\phi)}^{\frac{\pi}{2}} \sin^m\theta\cos\theta\, d\theta d\phi \; + \quad (3.17)$$

$$\frac{m+1}{2} \int_0^{\pi} \int_{\text{atan}(\tan\gamma\sin\phi)}^{\text{atan}(\tan\beta\sin\phi)} e^{-d/\lambda} \sin^m\theta\cos\theta\, d\theta d\phi \quad (3.18)$$

As erosional process of surface will be partially shielded, in this case, it is necessary to calculate amount of the flux that reaches beneath the scarp surface. In this condition, one may assume that the scarp surface is an infinite plane. The distance travelled by a radiation coming from the direction (θ, ϕ).

$$S_r(e,\beta) = \frac{m+1}{2\pi} \int_0^{\pi} \int_{\text{atan}(\tan\beta\sin\phi)}^{\pi/2} e^{-d_-/\lambda} \sin^m\theta\cos\theta\, d\theta d\phi \quad (3.19)$$

$$\frac{m+1}{2\pi} \int_0^{\pi} \int_0^{\pi/2} e^{-d_+/\lambda} \sin^n\theta\cos\theta\, d\theta d\phi \quad (3.20)$$

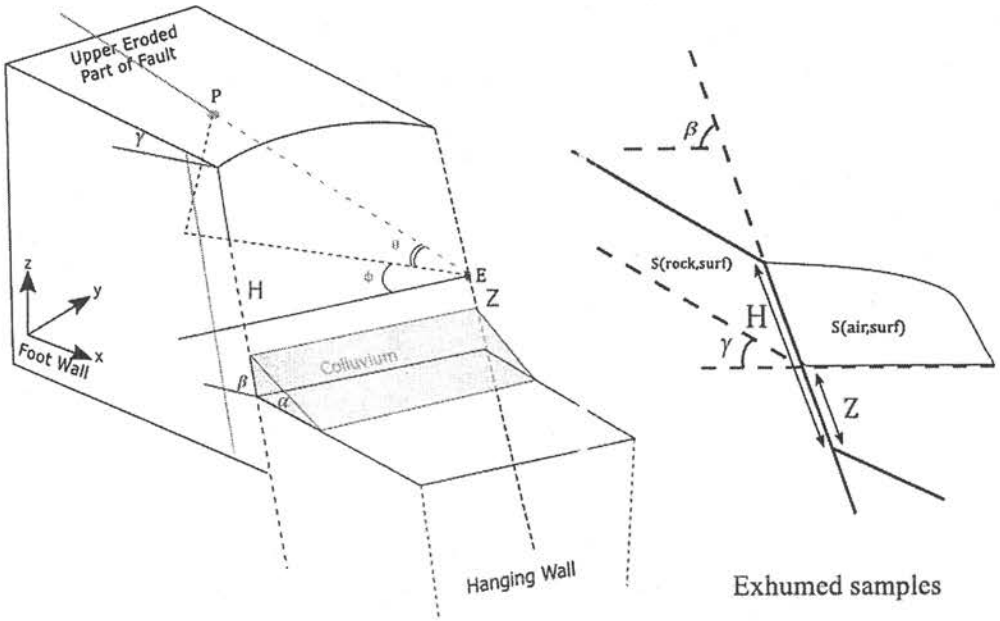

Figure 3.7: Exhumed samples receive cosmic rays going through the both air and through the rock (Modified after Schlagenhauf et.al, 2010).

As erosional process of surface will be partially shielded, in this case it is necessary to calculate amount of the flux that reaches beneath the scarp surface. In this condition, one may assume that the scarp surface is an infinite plane. The distance travelled by a radiation coming from the direction (θ, ϕ) as below

$$if\ 0 \leq \phi \leq \pi \tag{3.21}$$

$$d_{-} = \frac{e}{sin\theta\ cos\beta - cos\theta\ sin\alpha\ sin\phi} \tag{3.22}$$

$$if\ 0 \leq \phi \leq 2\pi \tag{3.23}$$

$$d_{+} = \frac{e}{sin\theta\ cos\beta + cos\theta\ sin\beta\ sin\phi} \tag{3.24}$$

Then the corresponding scaling factor will be

$$S_r(e,\beta) = \frac{m+1}{2\pi} \int_0^{\pi} \int_{\text{atan}(tan\beta\ sin\phi)}^{\pi/2} e^{-d_{-}/\lambda} \quad sin^m\theta\ cos\theta\ d\theta d\phi \tag{3.25}$$

$$+ \frac{m+1}{2\pi} \int_0^{\pi} \int_0^{\pi/2} e^{-d_{+}/\lambda} sin^m\theta\ cos\theta\ d\theta d\phi \tag{3.26}$$

$$+ S_r(e,\beta) \approx S_e\ exp(-e/\Lambda_e) \tag{3.27}$$

4. EARTHQUAKE MODELS

Using cosmic-ray surface exposure dating of a well-preserved limestone fault scarp facilitates us to attain information, which reveals a seismic history scenario of faulting events and identifies past major earthquakes, recurrence interval of major earthquakes and slip rates of fault zone. When secondary cosmic rays interact with surface (Figure 4.1), it starts to accumulate cosmogenic isotopes. As the effects of spallation reactions decrease through the depth of surface, the accumulation of ^{36}Cl decreases, as well.

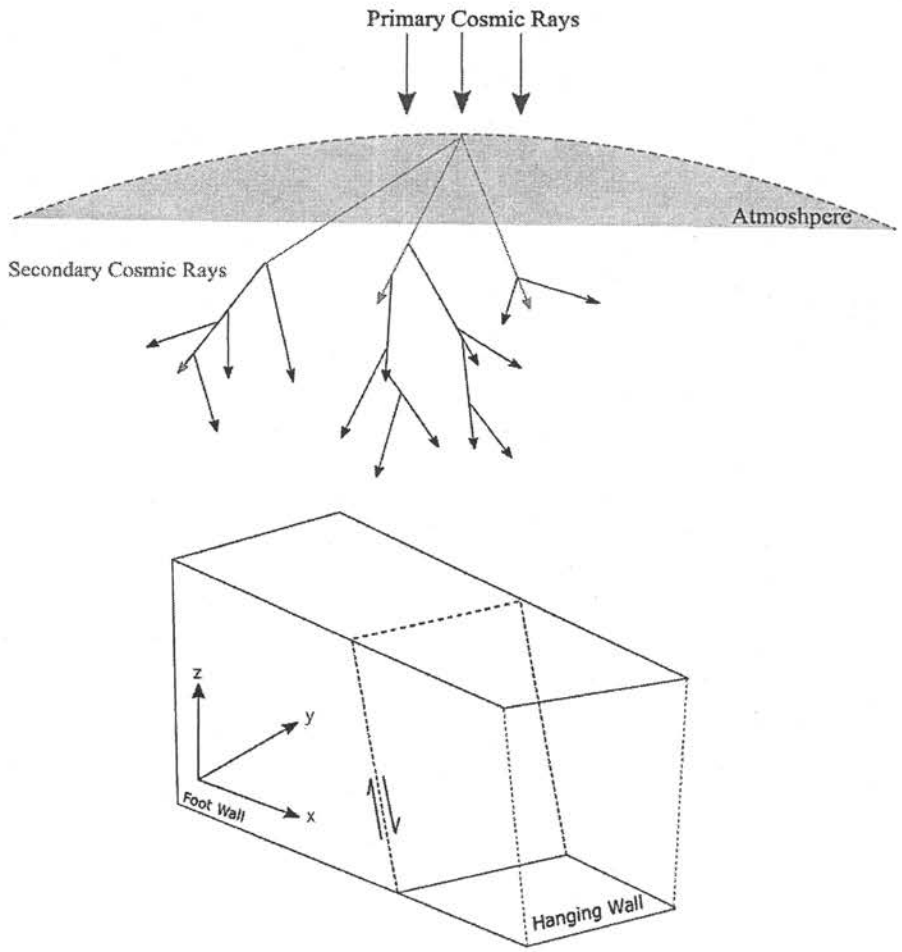

Figure 4.1: Interaction of secondary cosmic with a fault block before a rupture.

Three major events scenarios were created in order to comprehend natural processes. In this scenario, three events occurred at different times and all of those events

caused 2 m slip in random times. The exponential concentrations of this profile resulting of several different processes. Due to certain differentiation, those major discontinuities of ^{36}Cl concentration can be identified both sample concentration probability density functions (pdf) from AMS measurements and visual observation (Schlagenhauf et al., 2011).

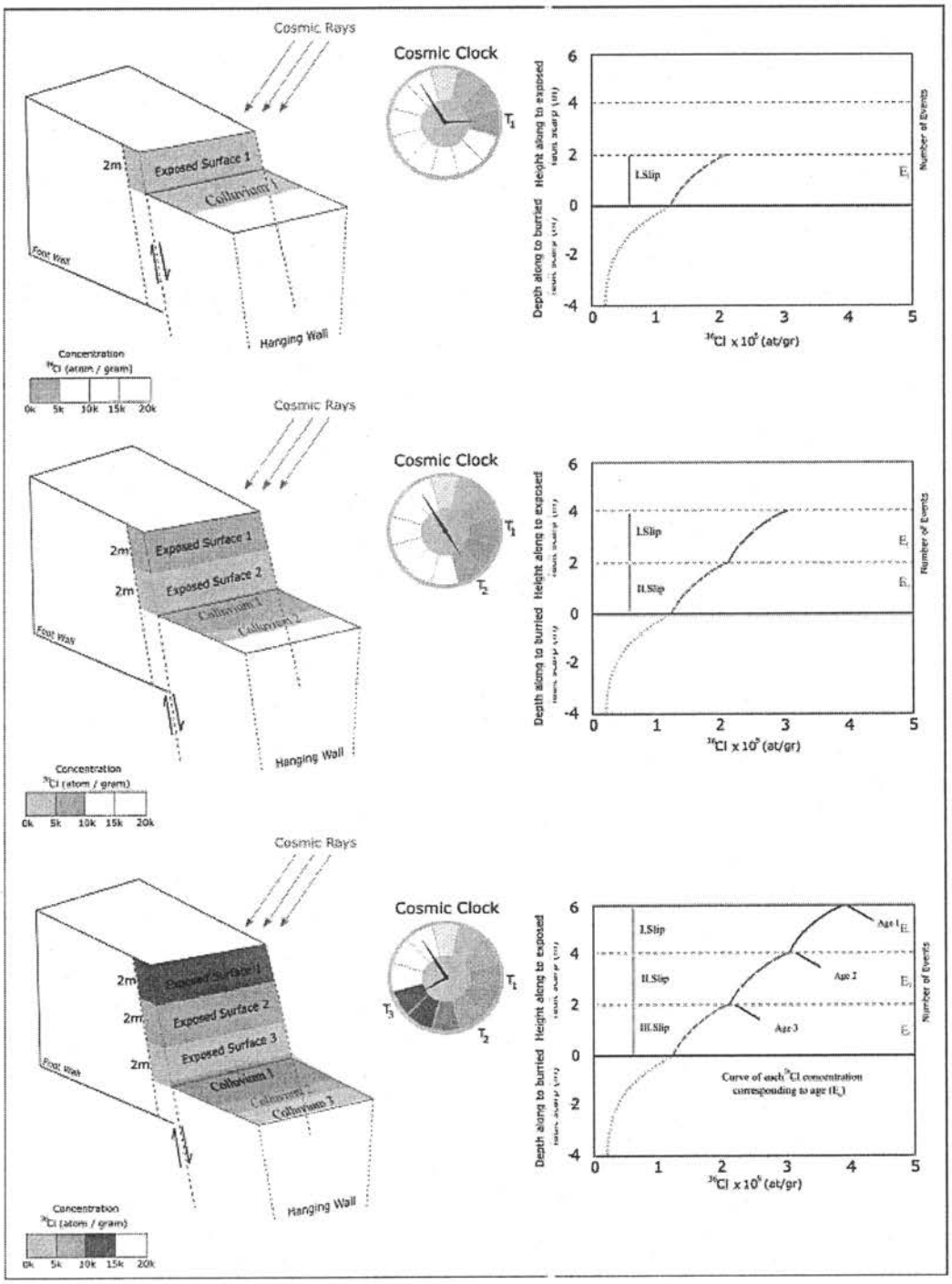

Figure 4.2: Representative illustration of three different major events.

The part of fault scarp exposed by each major events and their ^{36}Cl abundance of samples, which come from below colluvial wedge, are affected by pre-exposure

history. In addition to that, concentrations of cosmic isotopes depend on depth due to relative contributions of various processes that produce terrestrial in situ cosmogenic nuclides. When a large earthquake happens, part of the scarp residing under the surface exposed. Thereafter, that new part of the scarp starts to accumulate cosmic ^{36}Cl isotopes constant rate. In order to make robust evaluation of the sum of total amount of concentration, one should consider both ^{36}Cl produced under the surface before to exposure and the isotopes accumulated at the surface. As a result of that variation of concentration profile of ^{36}Cl along with its scarp, it shows series of discontinuities which is characteristic distribution of different events (Benedetti et.al, 2013). As it is seen in Figure 4.3, there are three different events, which caused same amount of slip at the same intervals. Each major event leaded to 2 m slip in 2 kyr. That is the easiest and the most perceptible case of the scenario according to the approach found in literature (Palumbo et.al 2004; Schlagenhauf et al., 2010).

It is shown in this section, the codes, which were developed by Schlagenhauf et.al (2010), generate models for the seismic history of faults and help to quantify the uncertainties in the number, ages, and slip rates of the past earthquakes. Moreover, codes contain all of the production rates of different elements and reactions. To be able to run Matlab program, one should put certain parameters in codes such as height of the fault scarp, colluvium dip, scarp dip, upper scarp dip; density of colluvium and samples. Due to production rate variations through elevation of study area, especially low latitudes it is difficult to recover earthquake timing. The shielding effects are completely dependent of geometry of the study area. As for colluvium thickness and its cover has very important effects on contribution of ^{36}Cl concentrations. After all of these factors were taken into account, I, then applied the code to a data set acquired on the Mezarlık fault scarp.

In order to generate ^{36}Cl concentration profiles, basic parameters were used. H refers to height of the scarp, α dip of colluvium is $16^{\circ} \pm 3$, β dip of scarp is $59^{\circ} \pm 3$ and γ dip of the older fault section is $29^{\circ} \pm 2$. Mean density of samples is 2.53 gr/cm^{-3} and mean density of the colluvium samples 1.5 gr/cm^{-3} (Figure 4.4). It was assumed that there were no significant erosion that had affected the fault scarp before. Elementary production rates for limestone used in these models provided in Appendix A. The other parameters used in the calculation of modelling were taken exactly same from Benedetti et al. (2013). However, only ^{36}Cl production rate from spallation of

calcium was taken from Schimmelpfennig et a. (2011). In order to avoid scaling problems, it

was preferred using local production rates (Schlagenhauf et al., 2011). Thus, models that are more efficient could be achieved. With increasing depth spallation reactions loses its dominance. As a result of that the chemical composition of all of samples indicate that element calcium (Ca) is responsible for 99% percent the total production of cosmic ^{36}Cl isotopes.

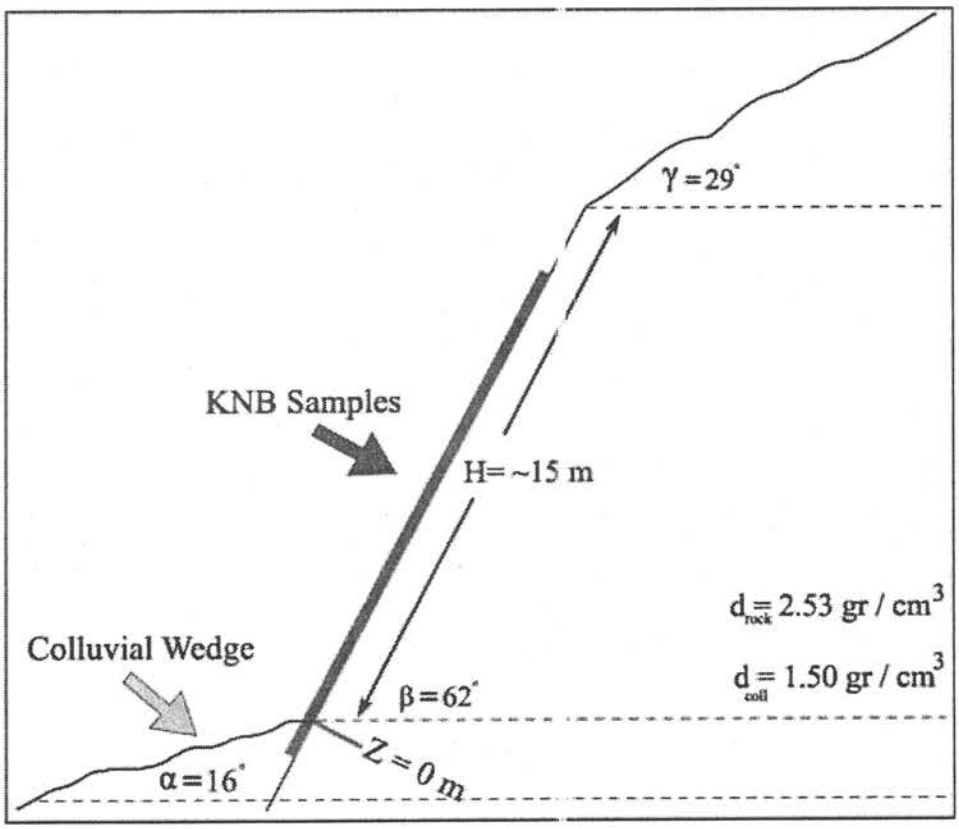

Figure 4.3: The Mezarlık fault geometry along with sampled section of the scarp. Blue line shows sampling part.

Even though other elements such as potassium (K), titanium (Ti), and iron (Fe) show affection of the concentration, they are not as efficient as calcium (Ca) in this study's data set. Each type of production rates at sea level high latitude for different particles and attenuation lengths are taken from literature.

The data set of sampled profile KNB of the Mezarlık Fault and position of samples on the position of the samples on the fault scarp and along with their ^{36}Cl concentration provided tables, which are in Appendix A.

Considerations of three major events as three different displacements at different periods, Figure 4.5 was produced. According to the first model, it is clearly seen that

at least three major events were occurred due to Each distinct steps indicate major evets in the model. Among these events, the first event occurred 18.7 ka and it caused 3.08 meters slip. The second event occurred 3 ka later after the first one, 15 ka and in addition to these, the last event occurred 10.8 subsequently. The last two events also caused 2.0 m and 6.52 m slip.

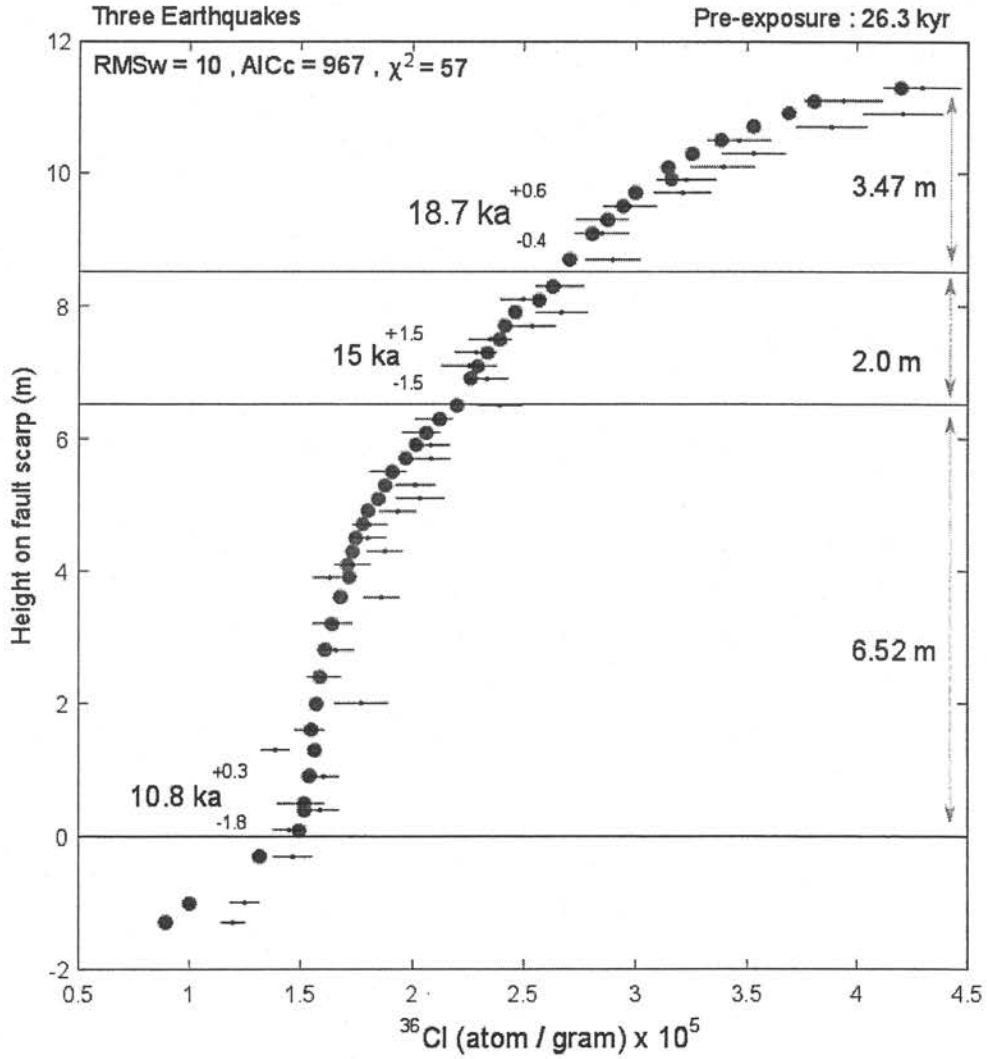

Figure 4.4: Three major events.

The youngest event probably cannot be true, as I do not have enough samples to correlate the results. When I receive the results of other samples, they might provide much more reliable information about activity of the Mezarlık fault.

Considering four major events situation as four different displacements at different time Figure 4.5 was generated. Although absence of high resolution dataset between 5 meters and -2 meters, there might be one more probable major event. The first event caused 3.08 (+1.5 / -0.4) m slip and 18.7 (+0.6 / - 0.4) ka; the second event 2.0 (+0.2 / -0.15) m slip and it occurred 15 ka (+1.5 / - 1.5); the third event 2.72 (+0.3 / -

0.5) m slip and it occurred 12.8 ka (+ 1.1 / - 0.9) and the last event is the fourth event caused 3.80 (+0.2 / - 0.7) m slip and it occurred 10 (+ 0.3 / - 1.8) ka. . In this model, we can see that four different events occurred on the Mezarlık fault. Unlike from the previous model, it can be interpreted the youngest event as two separate events. These last two events occurred 12.8 ka and 10 ka; the amount of slips 2.72 m and 3.80 m respectively.

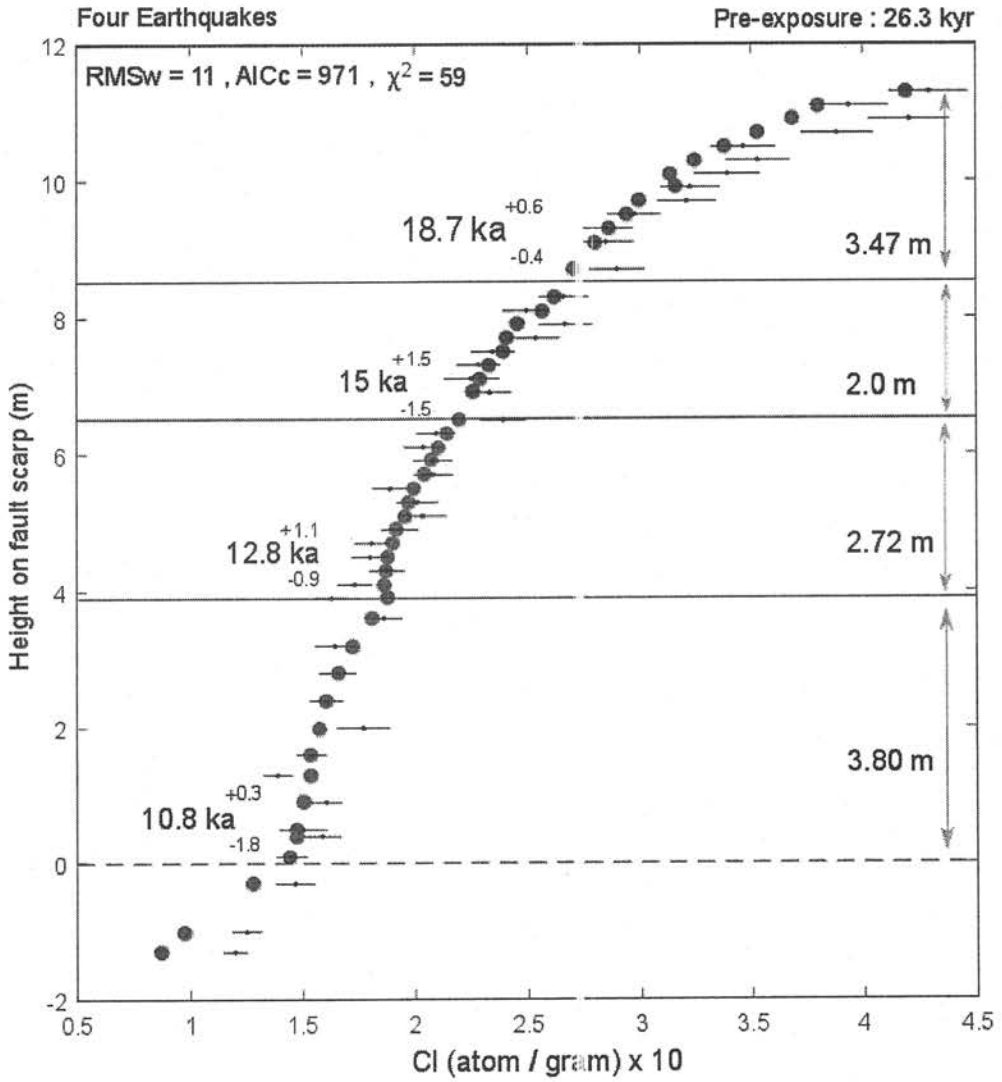

Figure 4.5: Four major events.

In this model, we can see that four different events occurred on the Mezarlık fault. However, younger event still has highest displacement from others. The first event caused 3.47(+1.5 / -0.4) m slip and 18.7 (+0.6 / - 0.4) ka; the second event 2.0 (+0.2 / -0.15) m slip and it occurred 15 ka (+1.5 / - 1.5); the third event 2.72 (+0.3 / - 0.5) m slip and it occurred 12.8 ka (+ 1.1 / - 0.9) and the last event is the fourth event caused 3.80 (+0.2 / - 0.7) m slip and it occurred 10 (+ 0.3 / - 1.8) ka. Unlike from the

previous model, it can be interpreted the youngest event as two separate events. These last two events occurred 12.8 ka and 10 ka; the amount of slips 2.72 m and 3.80 m respectively.

4.1 Moment Magnitudes

It was focused on maximum vertical displacement method due to data sets that were generated indicate primarily vertical movement of the fault scarp. The importance of moment magnitude is direct relationship between geometry and physical properties of faults. After calculation amounts of slips of the events that caused major displacement, one can use empirical relationship between slip and moment magnitudes. Therefore, in order to estimate magnitudes of earthquakes, maximum vertical displacement method was used (Wells and Coppersmith, 1994). Moreover, through this estimation of moment magnitudes of each major event, one can calculate surface rupture length values. It must be pointed out that there are many sources of error contains in those empirical equations.

$$M_w = 6.61 \mp 0.09 + 0.71 \mp 0.15 \; log(MD) \qquad (4.1)$$

In the empirical equations Mw refers to moment magnitude, MD is maximum displacement and AD is average displacement.

These two different cases and using their displacement values, different results were obtained. The maximum vertical displacement method for three and four events cases indicate that magnitudes of the earthquakes which can produce the Mezarlık fault scarp varies between 6.8 (+0.2 / - 0.1) and 7.2 (+0.2 / - 0.4) moment magnitudes.

5. CONCLUSION

In order to get information about seismic hazards, fault parameters such as moment magnitude, rupture length, slip rate and recurrence interval are very important in active tectonic studies. It is recovered that the Late Pleistocene and Early Holocene earthquake history of the normal fault in Datça Peninsula in the western Turkey. 128 samples were collected from the well-preserved limestone scarps of the Mezarlık fault. Nevertheless, only 49 out of 128 samples were modelled ^{36}Cl concentrations to obtain its seismic exhumation history. Using cosmic-ray surface exposure dating of a well-preserved limestone fault scarp facilitates us to attain information, which reveals a seismic history scenario of faulting events and identifies past major earthquakes, recurrence interval of major earthquakes and slip rates of fault zone. The limitations and uncertainties of models were discussed in 2010 Schlagenhauf et.al, in details.

Modelling of ^{36}Cl concentration data collected from the Knidos Fault Zone give clues about Post-Glacial seismic activity. Furthermore, it can help to interpret evolution of landform resulting from interaction of tectonic and surface processes. The distribution of concentration of ^{36}Cl of the Mezarlık fault indicates that there might have been at least three, four or more events occurred. The slip rates on the Mezarlık fault have varied through time. Based on the goodness of fit estimations, three and four events occurred between 20 and 10 kyr. This period indicates Post-Glacial exposure of the fault scarp as it is observed other localities in the Mediterranean Region. Modelling of cosmic isotope concentration of fault scarps allow us to understand the temporal pattern of past fault activity. Even though modelling allows identifying large slip events, it cannot discriminate whether those events are single or multiple. The model results are enormously dependent geometry of the fault and study site. Moreover, displacement uncertainty is ± ~0.2 m and age uncertainty of ± 0.5–1.0 kyr. Consequently, the amount of displacement is in their maximum values while the number of earthquake is minimum. In addition to that, the age of the event are estimated roughly. The slip histories modelled via concentrations

of ^{36}Cl indicate that at least three or more events occurred on the Mezarlık fault within the past 20 kyr; over 10 meters of displacement took place between early Holocene and late Pleistocene. Through maximum displacement method calculations, the earthquake magnitudes occurred on the Mezarlık fault were between 6.2 and 7.2. Citing that case and others as evidence of seismic hazard to the Knidos Fault Zone. When considering that there are only 49 samples out of 128 at present, we do not have high resolution of dataset recent activity of the Mezarlık fault. Due to absence of results of ^{36}Cl concentration of samples, we do not have significant evidences for middle-Holocene earthquake activity. However, there are 79 more samples by the time I receive result of AMS concentrations that I can use them in future.

REFERENCES

Akaike, H. (1974). A new look at the statistical model identification, *IEEE Trans. Automatic Contl.* ***19(6)***, 716–723.

Altunel, E., Stewart, I., Barka, A., Piccardi, L. (2001). Earthquake Faulting at Ancient Cnidus, SW Turkey, *Turkish Journal of Earth Sciences (Turkish J. Earth Sci.).* ***12,*** 2003, pp. 137-151.

Benedetti, L., R. Finkel, D. Papanastassiou, G. King, R. Armijo, F. Ryerson, D. Farber, and F. Flerit. (2002), Post-glacial slip history of the Sparta fault (Greece) determined by 36Cl cosmogenic dating: Evidence for non-periodic earthquakes. *Geophys. Res. Lett.*, ***29(8)***, doi: 10.1029/2001GL014510.

Benedetti, L., R. Finkel, G. King, R. Armijo, D. Papanastassiou, F. J. Ryerson, F. Flerit, D. Farber, and G. Stavrakakis. (2003). Motion of the Kaparelli fault (Greece) prior to the 1981 earthquake sequence determined from 36Cl cosmogenic dating, *Terra Nova*, ***15(2)***, 118–124.

Benedetti, L., I. Manighetti, Y. Gaudemer, R. Finkel, J. Malavieille, K. Pou, M. Arnold, G. Aumaître, D. Bourlès, and K. Keddadouche. (2013). Earthquake synchrony and clustering on Fucino faults (Central Italy) as revealed from in situ 36 Cl exposure dating, *J. Geophys. Res. Solid Earth*, ***118(9)***, 4948–4974.

Benedetti, L. C., and J. van der Woerd. (2014). Cosmogenic Nuclide Dating of Earthquakes, Faults, and Toppled Blocks, *Elements*, ***10(5)***, 357–361.

Burnham, K.P. and Anderson, D.R. (2002). *Model Selection and Multi- Model Inference: A practical Information-Theoretical Approach.* Springer Verlag, New York.

Carcaillet, J., Manighetti, I., Chauvel, C., Schlagenhauf, A. & Nicole, J.-M. (2008). Identifying past earthquakes on an active normal fault (Magnolia, Italy) from the chemical analysis of its exhumed carbonate fault plane, *Earth planet. Sci. Lett.*, ***271(1–4)***, 145–158.

Dirik, K. (2007). Neotectonic characteristics and seismicity of the Reşadiye Peninsula and surrounding area, southwest Anatolia. *Geological Bulletin of Turkey.* ***50(3)***, 130-149.

Gosse, J.C. and Phillips, F.M. (2001). Terrestrial in situ cosmogenic nuclides: theory and application, *Quater. Sci. Rev.*, ***20***, 1475–1560.

Marrero, S. (2012). *Calibration of Cosmogenic Chlorine-36.* (PhD Thesis). New Mexico Institute of Mining and Technology.

Mitchell, S. G., A. Matmon, P. R. Bierman, Y. Enzel, M. Caffee, and D. Rizzo. (2001). Displacement history of a limestone normal fault scarp,

northern Israel, from cosmogenic 36Cl, *J. Geophys. Res.*, ***106(B3)***, 4247–4264.

Stone, J.O., Allan, G.L., Fifield, L.K. & Cresswell, R.G. (1996). Cosmogenic chlorine-36 from calcium spallation, *Geochim. Cosmochim. Acta.*, ***60(4)***, 679–692.

Stone, J.O., Evans, J.M., Fifield, L.K., Allan, G.L. & Cresswell, R.G. (1998). Cosmogenic chlorine-36 production in calcite by muons, *Geochim. Cosmochim. Acta*, ***62(3)***, 433–454.

Stone, J.O. (2000). Air pressure and cosmogenic isotope production, *J. Geophys. Res.*, ***105(B10)***, 23,753–23,759.

Schimmelpfennig, I., Benedetti, L., Finkel, R., Pik, R., Blard, P.-H., Bourlès, D., Burnard, P. & Williams, A. (2009). Sources of in-situ 36Cl in basaltic rocks, implications for calibration of production rates, Quarter. Geochronology.

Schimmelpfennig, I., L. Benedetti, V. Garreta, R. Pik, P.-H. Blard, P. Burnard, D. Bourlès, R. Finkel, K. Ammon, and T. Dunai. (2011). Calibration of cosmogenic 36Cl production rates from Ca and K spallation in lava flows from Mt. Etna (38°N, Italy) and Payun Matru (36°S, Argentina), *Geochim. Cosmochim. Acta*, doi:10.1016/j.gca.2011.02.013.

Schlagenhauf, A., Gaudemer, Y., Benedetti, L., Manighetti, I., Palumbo, L., Schimmelpfennig, I., Finkel, R., Pou, K. (2010). Using in situ Chlorine-36 cosmonuclide to recover past earthquake histories on limestone normal fault scarps: a reappraisal of methodology and interpretations. *Geophys. J. Int.* doi:10.1111/j.1365-246X. 2010.04622.x.

Stone, J.O., Allan, G.L., Fifield, L.K. & Cresswell, R.G. (1996). Cosmogenic chlorine-36 from calcium spallation, *Geochim. Cosmochim. Acta.*, ***60(4)***, 679–692.

Wells, D. L., and K. J. Coppersmith. (1994). New empirical relationships among magnitude, rupture length, rupture width, and rupture area, and surface displacement, *Bull. Seism. Soc. Am.*, ***84***, 974-1002.

APPENDICES

APPENDIX A: Tables

Table A.1: AMS measurements first part.

Sample Name	(36Cl) AMS	Uncertainty
KNB-01	429237	17535
KNB-03	393781	17847
KNB-05	420495	17939
KNB-07	388406	16172
KNB-09	346484	14415
KNB-11	352951	14546
KNB-13	339249	14628
KNB-15	322665	13400
KNB-17	320956	13033
KNB-19	297507	12075
KNB-21	285184	11791
KNB-23	285040	12155
KNB-27	289906	12362
KNB-31	266205	10995
KNB-33	249579	10209
KNB-35	266986	11774
KNB-37	253772	10758
KNB-39	234946	9651
KNB-41	228606	9647
KNB-43	225534	12467
KNB-45	233606	9573
KNB-49R	239338	10098
KNB-51	209642	8545
KNB-53	203940	8835
KNB-55	208190	8735
KNB-57	208407	8784
KNB-59	189102	7924
KNB-61	201227	9253
KNB-63	203478	10842
KNB-65	193407	8301
KNB-67	180889	7873
KNB-69	180123	8175
KNB-71	187622	8076
KNB-73	173245	8002
KNB-75	162969	7401
KNB-78	186118	8124
KNB-82	164251	8905
KNB-86	165599	8240
KNB-90	160534	7623
KNB-94	177111	11994
KNB-98	154017	6683

Table A.2: AMS measurements of second part.

Sample Name	(36Cl) AMS	Uncertainty
KNB-98	154017	6683
KNB-101	138831	6613
KNB-105	160492	6922
KNB-109	150077	10718
KNB-110	158780	8374
KNB-113	144921	7122
KNB-117	146589	8703
KNB-125	124937	6584
KNB-128	119814	5541

Table A.3: Mean chemical composition of trace elements.

Name	Amount
As (ppm)	1.63
B (ppm)	0.000
Ba (ppm)	186.5
Be (ppm)	0.000
Bi (ppm)	0.000
Cd (ppm)	0.000
Ce (ppm)	0.97
Co (ppm)	0.9
Cr (ppm)	0.000
Cs (ppm)	0.3
Cu (ppm)	0.7
Dy (ppm)	0.1267
Er (ppm)	0.08
Eu (ppm)	0.025
Ga (ppm)	0.000
Gd (ppm)	0.14
Ge (ppm)	0.000
Hf (ppm)	0.000
Ho (ppm)	0.033
In (ppm)	0.000
La (ppm)	0.67
Li (ppm)	0.000
Lu (ppm)	0.02
Mo (ppm)	0.13
Nb (ppm)	0.35
Nd (ppm)	0.433
Ni (ppm)	5.6
Pb (ppm)	2.467
Pr (ppm)	0.103
Rb (ppm)	0.967
Sb (ppm)	0.1
Sm (ppm)	0.135
Sn (ppm)	0.000
Sr (ppm)	198.27
Ta (ppm)	0.000

Table A.4: Mean chemical composition major and trace elements.

Name	Amount
Th (ppm)	0.5
Tm (ppm)	0.001
U (ppm)	2.7
V (ppm)	0.000
W (ppm)	0.000
Y (ppm)	1.000
Yb (ppm)	0.095
Zn (ppm)	21.7
Zr (ppm)	1.77
O,rock (ppm)	0.000
O,water (ppm)	0.000
Fe_2O_3(Fe) (%)	0.123
MnO(Mn) (%)	0.02
MgO(Mg) (%)	0.52
CaO(Ca) (%)	56.03
Na_2O(Na) (%)	0.01
K_2O(K) (%)	0.04
TiO_2(Ti) (%)	0.01
P_2O_5(P) (%)	0.02
H_2O_{tot}(H) (%)	0.333
S_{tot}(S) (%)	0.016
$CO_{2\ tot}$(C) (%)	44.358

Table A.5: Geographic information of the study area.

Fault	Site Name	Latitude	Longitude	Elevation
Mezarlık	KNB	N 36°41'9.30"	E 27°23'24.52"	95 ± 5 m

Table A.6: Geometrical and physical characteristics of the profile.

ρrock	ρcoll	α	β	γ	El_f	El_mu	H
2.53	1.5	16 ± 3	59 ± 3	29 ± 2	0.707	0.858	12.8 m

CIRRICULUM VITAE

Name Surname : Sefa ŞAHİN

Place and Date of Birth : İstanbul, 1984

E-Mail : sefasahin@gmail.com & sahinsefa@itu.edu.tr

EDUCATION

- **B.Sc.** : İstanbul University, Engineering Faculty, Geophysics Engineering Department. (2008-2012)
- **High School** : Bakırköy Lisesi , 2001

PUBLICATIONS, PRESENTATIONS AND PATENTS ON THE THESIS:

- Şahin, S., Yıldırım C., Sarıkaya M.A., Tüysüz,O., Genç, Ş.C., Aksoy M.E., Doksanaltı M.E., 2016: Reconstruction of the Earthquake History of Limestone Fault Scarps in Knidos Fault Zone Using in-situ Chlorine-36 Exposure Dating and "R" Programming Language. *European Geosciences Union General Assembly*, 17–22 April 2016, Vienna, Austria.